Chapter 20

HRMA Ghost Image Properties

Terrance J. Gaetz

20.1 Ghost Images – Geometry

Ghost images occur when photons reach the focal plane after missing the paraboloid or the hyperboloid of a given mirror pair. The ghost rays can be classified into the following types:

- nonreflected rays: missed both the P (paraboloid) and the H (hyperboloid) optics of a given mirror pair.
- P-ghosts: missed the P mirror.
- H-ghosts: missed the H mirror.

The HRMA was designed to suppress ghost images within $14'$ of the optical axis. This was accomplished by X-ray baffles at the location of the first thermal precollimator plate and X-ray baffles at the aft surface of the HRMA Central Aperture Plate (CAP). In addition, an X-ray baffle is needed in the P6 cavity. A description of the X-ray baffle design is given in Gaetz (1993).

The behavior of the ghost images can be understood qualitatively as follows. If a Wolter Type-I mirror pair were completely unbaffled, ghost rays would reach the focal plane even in the on-axis case. Individual mirror elements do not focus rays at the same location as a mirror pair: the paraboloidal mirror elements focus rays behind the mirror pair focal plane, while the hyperboloidal mirror elements focus rays ahead of the pair focal plane (see Figure 20.1)

Rays which are parallel to the optical axis and which hit the P optic will also reflect off the H optic (neglecting the effects of scattering and assuming a perfectly aligned system). Because the H optics are actually slightly over-long compared to the matching P optics, there is a slight range of off-axis angles (in the as-designed system) where rays hitting the P optic will continue to hit the H optic. Eventually, though, the off-axis angle becomes steep enough that rays hitting near the front of the P will be reflected too steeply to hit the H optic; such rays become ghost rays if they are not blocked (Figure 20.2). Rays which are parallel to the optical axis and hit the hyperboloid will reach the focal plane as ghost rays (in an unbaffled system) but well outside the the detector area; to lowest order, the radius of this H-ghost ring is half the radius of the mirror pair.

The behavior of the ghost images can be understood qualitatively by considering the reflection properties of individual paraboloid or hyperboloid mirrors. Consider a paraboloidal mirror element by itself (*i.e.*, in the absence of its companion hyperboloid); rays from an on-axis point source at infinity will produce an out-of-focus ring at the (mirror pair) focal plane. In this case, the focus of
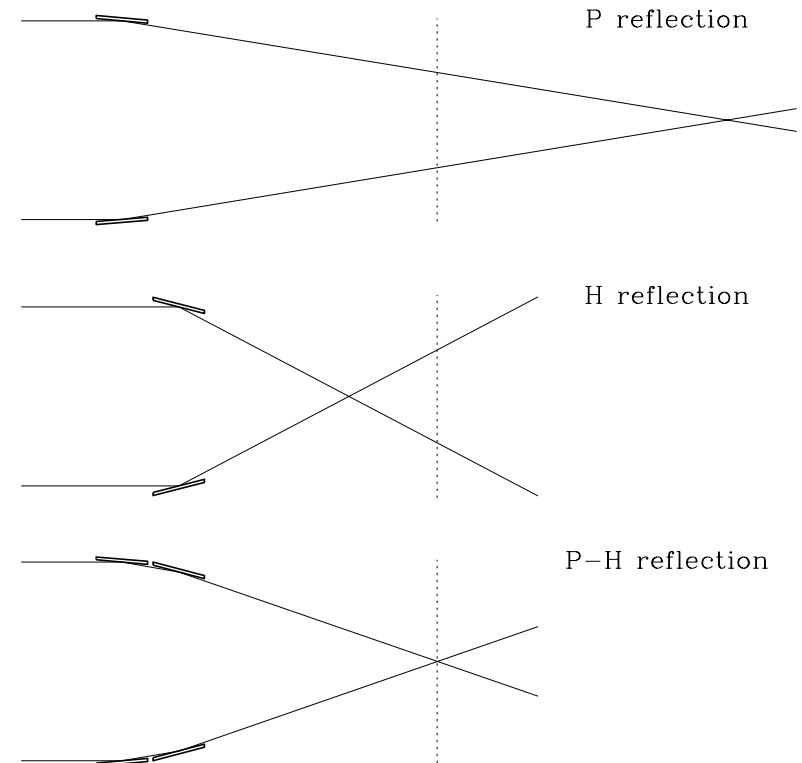

Figure 20.1: Schematic diagram of rays reflected from a single P or H mirror element compared to the P and H combination of the Wolter type I design. The dashed line indicates the focal plane for the mirror pair.

the optic is behind the system focus so that the $+Y$ portion of the out of focus ring is produced by the $+Y$ portion of the optic. A hyperboloidal mirror element by itself also produces an out of focus ring; however, because the hyperboloid focuses the rays ahead of the focal plane, the image is inverted and the $-Y$ portion of the image is produced by the $+Y$ portion of the optic. In reality, the on-axis rays which hit the P optic will also reflect from the companion H optic and reach the system focus. In the absence of baffles, rays which miss the P optic will hit the H optic and become single reflection H-ghosts, or miss both the P and H optics and become nonreflected ghosts. The HRMA baffles are designed to reject non-reflected ghost rays, and to prevent single reflection ghosts from hitting within the central $14'$ of the focal plane, while at the same time not vignetting doubly-reflected rays incident within $14'$ of the optical axis.
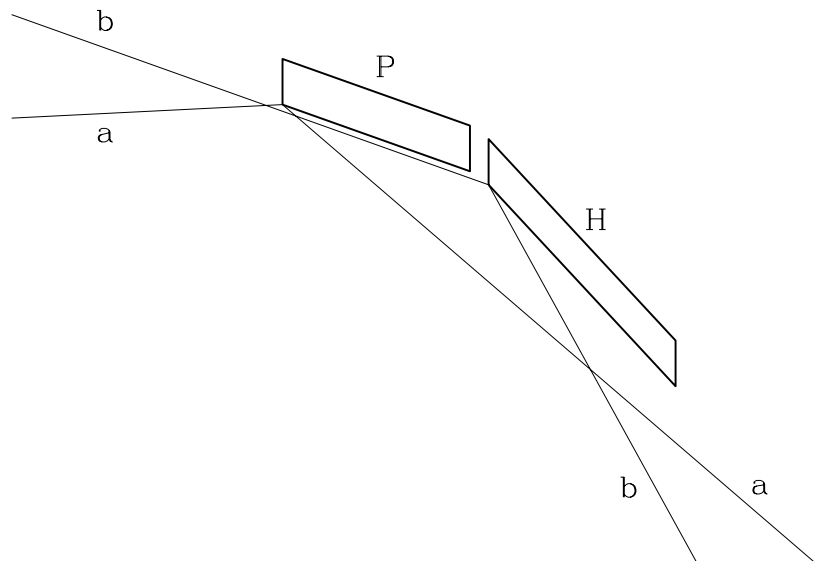
Figure 20.2: Schematic diagram of single reflection ghosts. Ray *a* strikes the parabola with too steep a positive slope and the reflected ray misses the aft end of the hyperbola becoming a "P ghost". Ray *b* is an example of an "H ghost".

Note that the finite length of the optics produces edges which vignette the rays. In the AXAF mirror design, the H optics are slightly over-long compared to the P optics: for perfect optics and perfect alignment, the set of rays parallel to the axis which illuminate the P optics are reflected and illuminate almost all of the companion H optics; however, a narrow band at the forward and aft end of each H optic is unilluminated.

As a source moves further and further off-axis, the rings of singly-reflected rays deforms inward (along the axis containing the source and the optical axis). The ring forms a cusp (cardioid-like) when the off-axis angle is comparable to the graze-angle of the mirror; thereafter, the ghost ring forms a double-loop (very much like a limaçon); both branches of the limaçon grow, and the smaller loop eventually crosses the optical axis unless appropriate X-ray baffles are in place (see Figure 20.3).

20.2   Ghost Baffle Design

In Figure 20.4, possible locations of X-ray baffles in Wolter type I systems are indicated, together with the vignetting constraints. The utility of ghost baffles at each of these locations is discussed by
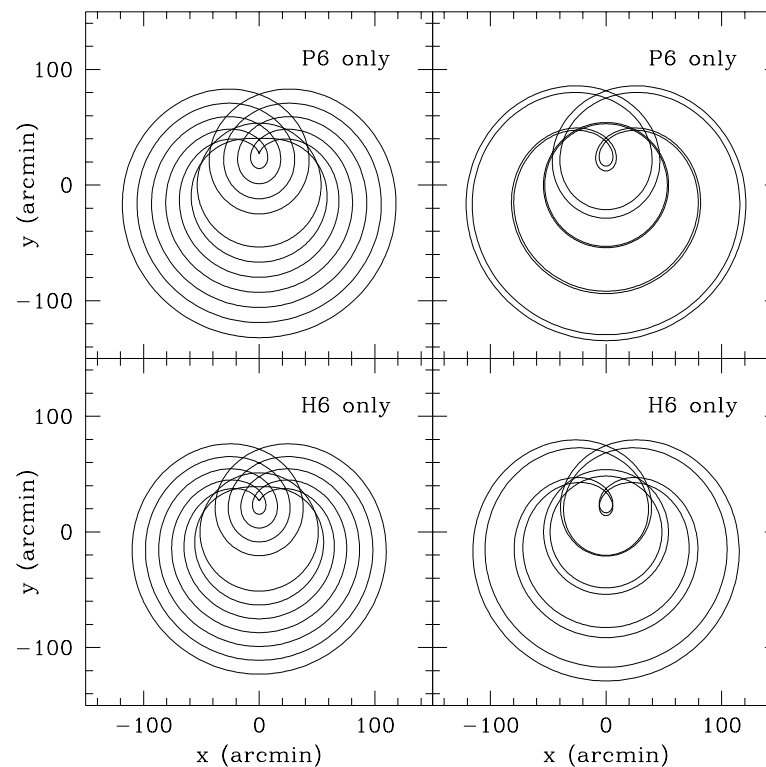
Figure 20.3: The left panels shows the images of rays from a point source at infinity and intercepting a mirror element at its midplane; curves are shown for source off-axis angles of 0, 12.5, 25, 37.5, 50, 62.5, and 75 arcmin. The right panels show the images of rays reflecting from the forward and aft edges of an individual mirror element; curves are shown for off-axis angles of 0, 37.5, and 75 arcmin. In each case only a single mirror element of the mirror pair is considered; the companion mirror element is absent, and the system is assumed to be unbaffled.

Austen and Torgenson (1980); they note that interior baffles (locations I_P and I_H are preferable, but baffling at F, C, or A is usually mechanically more practical. The baffles at the the A position serve to exclude ghost rays *outside* some radius from the optical axis, so they are not relevant to the problem of excluding ghost rays near the optical axis. The original ghost baffle design included baffles only at F and C; this design would not meet the requirement of the AXAF-I *Projects Requirement Document* (PRD) *Level II* (originally a *keep-out* zone of 15′), and it was

suggested that the requirement be relaxed. Gaetz (1993) showed that the addition of a baffle at the I_P position for P6 would allow the ghost exclusion requirement to be met; the final baffle design included a P6 interior baffle. Based on subsequent manufacturing tolerance concerns, the PRD *Level II* requirement was relaxed to $14'$ from the optical axis. In the following, we briefly discuss the baffling of P-ghosts, H-ghosts, and the vignetting implications.
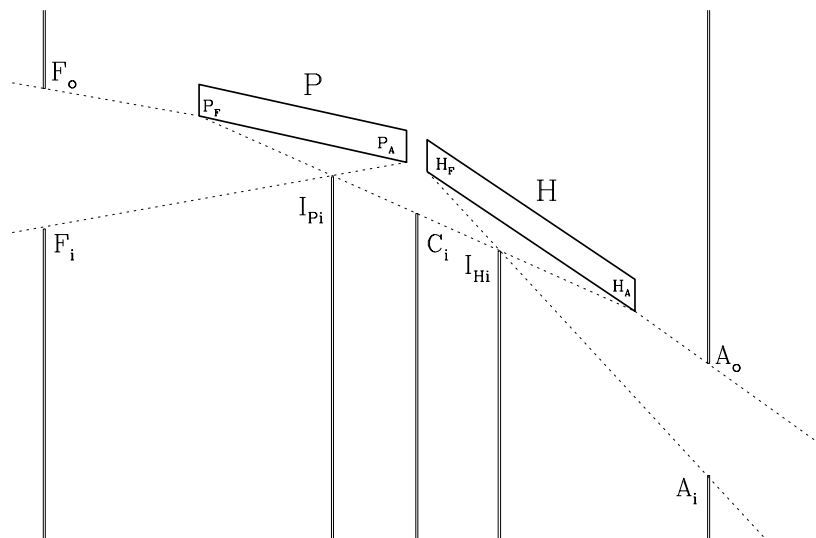

Figure 20.4: Schematic diagram of baffles for Wolter type I optics. The dashed lines originating at the forward and aft ends of the optics indicate the vignetting angles. The dashed line connecting the forward edge of the paraboloid (P) to the aft edge of the hyperboloid (H) indicates a limiting "good" ray. Potential baffle locations are forward of the optics (F), between the P and H (C), aft of the optics (A), interior to the paraboloid (I_P), or interior to the hyperboloid (I_H).

20.2.1 Control of Single Reflection Ghosts

The limiting H ghost ray is determined by baffle F_i and either I_{Pi} or C_i. In the AXAF-I HRMA design, baffling at F_i, F_o, and C_i works for the outer three shells (P1H1, P3H3, and P4H4), but is not adequate for the innermost shell (P6H6). However, as noted above, it turns out that a baffle at the location I_{Pi} enables the simultaneous vignetting/ghost ray requirements to be met, at least for ideal conditions; Figure 20.5 schematically indicates how the ghost baffle system works.

The addition of a baffle at I_P improves the control of H ghosts by reducing magnitude of the slope of the limiting ray for a given choice of vignetting angle θ_{Vo}; the degree of relief is limited by the need for the baffle to avoid the $F_i - P_A$ vignetting cone and the $P_F - H_A$ cone. Figure 20.6 schematically indicates how the ghost baffle system works.
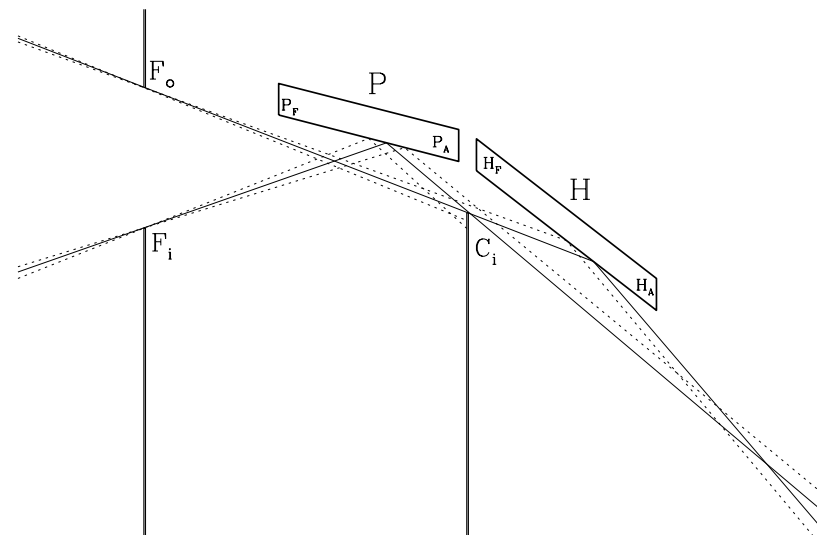
Figure 20.5: Control of ghost rays using baffles at F_i, F_o, and C_i. The P ghosts are controlled by the baffles F_i and C_i. The solid curve touching F_i indicates the limiting P ghost ray: steeper rays are blocked by the baffle C_i; shallower rays have a shallower angles after reflection and intercept the focal plane further out than the limiting ray. H ghosts are controlled by the baffles F_o and C_i. The solid curve through F_o indicates a limiting ghost ray: steeper rays are blocked by C_i; shallower rays have a steeper angles after reflection and intercept the focal plane further out than the limiting ray.

20.3 HSI Images of Ghosts

Ghost images are evident in the HSI off-axis images for angles $25'$ and greater. The basic features in the $30'$ off-axis images are shown in Figure 20.7

In Table 20.1, the off-axis HSI images which include P6 or H6 ghosts are listed.

At the angles for which HSI images were obtained, only single reflection P6 or H6 ghosts are visible. In the $25'$ off-axis images at Ti-Kα and Fe-Kα (Figure 20.9), part of the H6 loop (lower left corner of each image) is occulted by one of the cusps of the HSI mask. The full inner part of the H6 loop is visible in the $25'$ C-Kα image because the image is centered near the top of the detector; in this case most of one of the large lobes is lost. The Al-Kα image (MP6 only) is at about $24'$ off-axis, and the H6 ghost is in the problem of cusping. (Note that the off-axis direction also differs by $90°$ from the other images.) Comparing the difference between the image at $\sim 24'$ (H6 ghost image cusping, and hasn't yet reached the direct image) *versus* the images at $\sim 25'$ (ghost image forms a loop passing through the direct image) indicates that the ghost images in this angle range provide a sensitive measure of the actual angle the HRMA makes with the beamline axis.
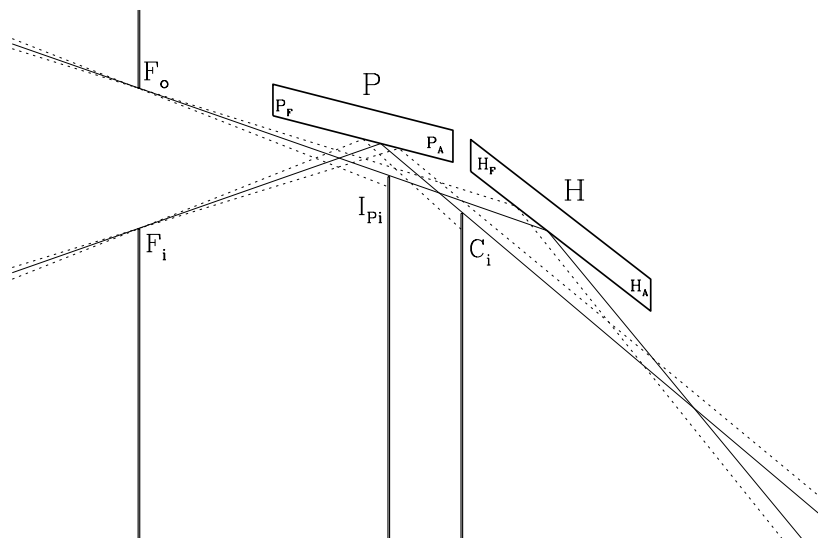
Figure 20.6: Control of ghost rays using baffles at F_i, F_o, I_{Pi}, and C_i. The P ghosts are controlled as in Figure 20.5. The H ghosts are controlled by the baffles F_o and I_{Pi}. The solid curve again indicates a limiting ghost ray: steeper rays are blocked by I_{Pi}; shallower rays have a steeper angle after reflection and intercept the focal plane further out than the limiting ray.

Table 20.1: Phase 1 Off-Axis Images with P6 or H6 ghosts

TRW ID	RunID	Energy (keV)	Shell	nominal pitch (′)	nominal yaw (′)	defocus (mm)	Counts
E-IXH-PI-6.006	110701	0.277	HRMA	−21.21	21.21	44.7368	32438
E-IXH-PI-21.006	111089	4.51	HRMA	−21.21	21.21	44.7368	58039
E-IXH-PI-11.006	110893	6.4	HRMA	−21.21	21.21	44.7368	282273
E-IXH-PI-6.005	110700	0.277	HRMA	−17.68	17.68	31.1065	48864
E-IXH-PI-52.001	111765	1.486	6	16.42	17.68	85.0136	98126
E-IXH-PI-21.005	111088	4.51	HRMA	−17.68	17.68	31.1065	56639
E-IXH-PI-11.005	110892	6.4	HRMA	−17.68	17.68	31.1065	128426

20.4   Determination of Off-axis Angle Using Ghosts

The sampled angles are particularly interesting in that they occur near the angles at which the P6 and H6 ghosts cusp and turn into loops. The fact that the both the direct image and the H6
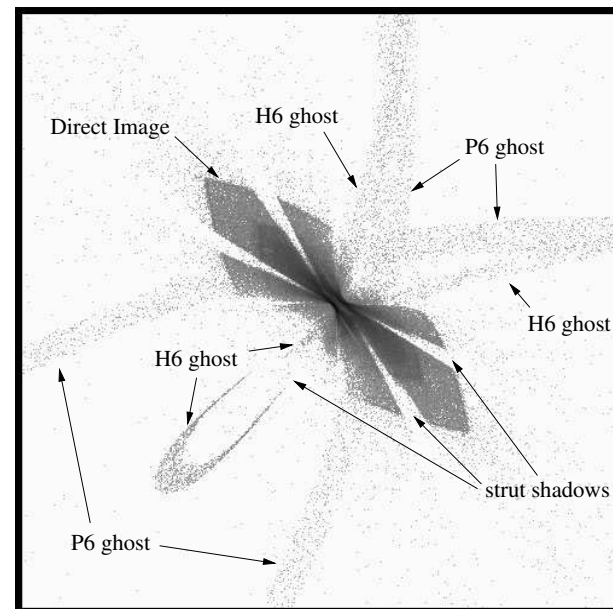

Figure 20.7: Off-axis image with ghosts. (Simulation of E-IXH-PI-11.006, runid 110893; Fe-Kα, 30′ off-axis.). At this angle, the single-reflection P ghost and single reflection H ghost can be readily discerned.

ghost loop are visible at the same time make these images useful for measuring the actual off-axis angle of the MP6 shell relative to the facility optical axis. The anomalies of the line PRF relative to the simulated line width suggest that the assumed Initial Actuator Position (IAP) of the HRMA may be off by $\sim$1/4 arcmin in yaw from the best value based on available records. The simulated images at 25′ and 30′ off-axis also suggest that the IAP may be systematically in error by an amount of that order.

The size of the H6 ghost loop and its position are sensitive indicators for the magnitude of the off-axis angle, θ; it can be estimated to within $\sim\pm0.05'$. The azimuth of the off-axis angle, ϕ, is trickier to determine; accurate evaluation involves evaluation of subtle variations in feature locations as the azimuth varies on a scale of degrees or less. In Figure 20.10, typical critical features are indicated; Figure 20.11, simulations varying θ and ϕ are presented.

The determination of the HRMA orientation by this technique is currently ongoing; results will be presented as they become available.
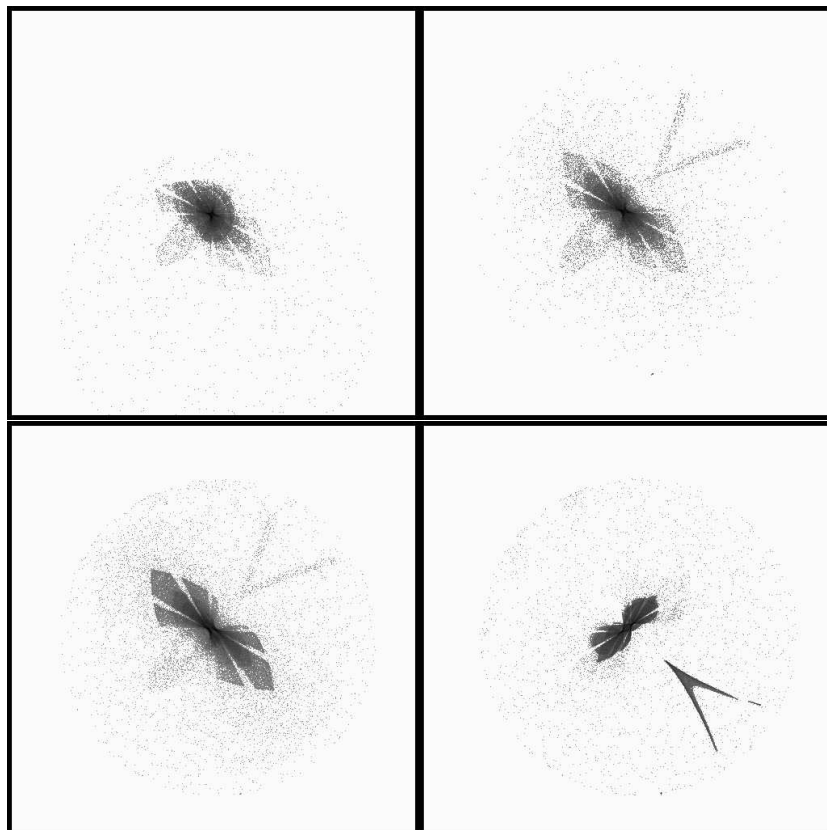
Figure 20.8: HSI images of ghosts at 25′ off-axis. Upper left: C-Kα (E-IXH-PI-6.005, runid 110700, 48864 counts) Upper right: Ti-Kα (E-IXH-PI-21.005, runid 111088, 56639 counts) Lower left: Fe-Kα (E-IXH-PI-21.005, runid 110892, 128426 counts) Lower right: Al-Kα (E-IXH-PI-52.001, runid 111765, 98126 counts) The image at Al-Kα was taken using the quadrant shutters to isolate mirror shell 6; because of actuator constraints, the off-axis angle was closer to 24′ off-axis, which is why the P-ghost has not formed a loop yet. In addition, the azimuth for the Al-Kα exposure differed by 90° from that used for the other energies.
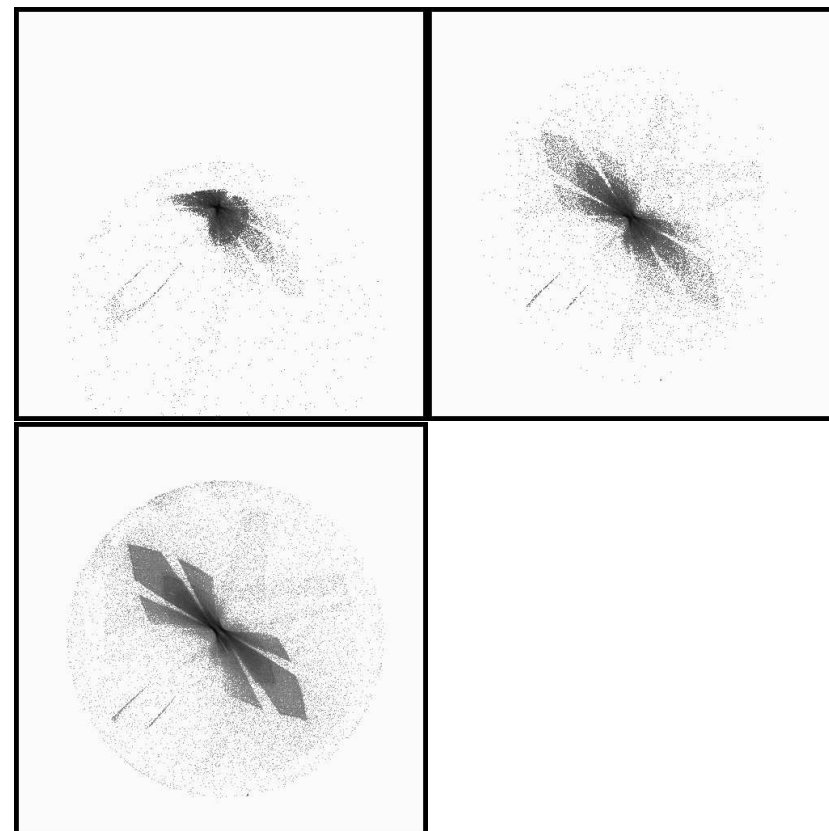

Figure 20.9: HSI full HRMA images of ghosts at 30′ off-axis. Upper left: C-Kα (E-IXH-PI-6.006, runid 110701, 32438 counts) Upper right: Ti-Kα (E-IXH-PI-21.006, runid 111089, 58039 counts) Lower left: Fe-Kα (E-IXH-PI-21.006, runid 110893, 282273 counts) Note that one of the cusps of the HSI mask occults part of the H6 ghost loop in the lower right of the Ti-Kα and Fe-Kα images.
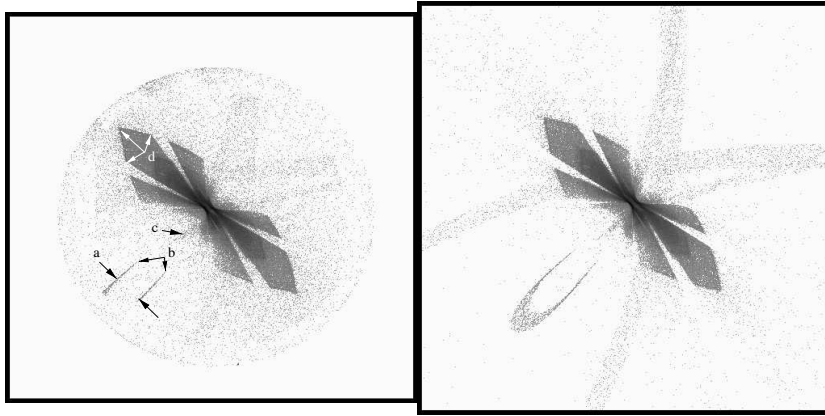
Figure 20.10: Determination of off-axis angle using the ghost in the 30′ off-axis Fe-α HSI image (E-IXH-PI-11.006, runid 110893). The planned angle was $\theta = 30'$, $\phi = -45°$. The value calculated from the actuator readings and relative to IAP7c2 is $\theta = 30.01952'$, $\phi = -45.0351°$. Top. The ghost loop is truncated lower left by the HSI mask cusp. The distance a is sensitive to the magnitude of the off-axis angle. The features b, c, and d help to refine the direction of the off-axis angle. Bottom. Simulation, ($\theta = 30.3039'$, $\phi = -44.75°$), almost matches the HSI image. The smaller ghost loop comes from one of the twelve open slots of the P6H6 optic; the gaps adjacent to feature b are produced by the support strut shadows. Feature c is the image of the next segment just beginning to appear. A large second ghost loop is also visible as a faint large loop.
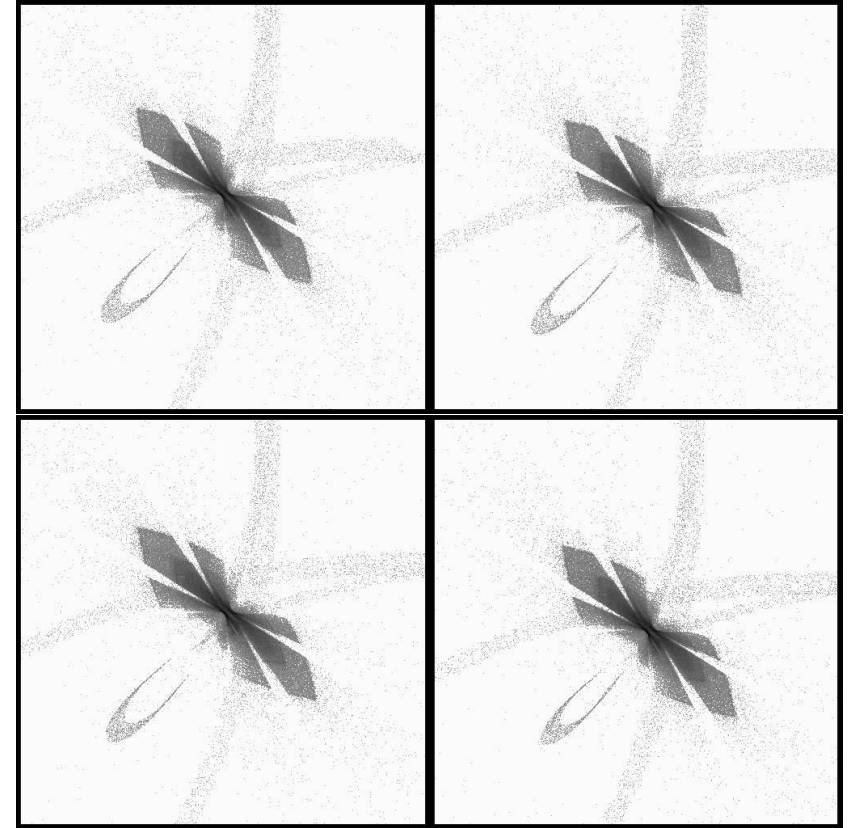
Figure 20.11: Top Left: $\theta = 30.3038'$, $\phi = -44°$ (Pitch, yaw = $[-21.0510', 21.7990']$). Top Right: $\theta = 30.3038'$, $\phi = -44.5°$ (Pitch, yaw = $[-21.2400', 21.6140']$). Bottom Left: $\theta = 30.3038'$, $\phi = -45°$ (Pitch, yaw = $[-21.4280', 21.4280']$). Bottom Right: $\theta = 30.0921'$, $\phi = -44.3618°$ (Pitch, yaw = $[-21.0400', 21.5140']$). Simulations for varying θ and ϕ. Comparing the bottom right figure with the others, it is evident that the width at a (see Figure 20.10) is sensitive to the off-axis angle θ; we estimate that the width of this feature restricts the value of θ to about $30.3' \pm 0.05$. Note also that as θ becomes more negative, the "horns" (feature b) on the smaller loop shift systematically. The feature c (see Fig. 1) shifts systematically with ϕ. The relative lengths of the segments at c also vary systematically. These features allow the value of ϕ to be estimated as about $44.675° \pm 0.15$.